Effective Structural Impact Detection and Localization Using Deep Learning and Information Fusion with Limited Sensors

Yuguang Fu[1], Zixin Wang[2], Amin Maghareh[2], Shirley Dyke*[2], Mohammad Jahanshahi[2], Adnan Shahriar[3]

[1] *School of Civil and Environmental Engineering, Nanyang Technological University, Singapore, 639798;*

[2] *Lyles School of Civil Engineering, Purdue University, West Lafayette, IN 47907, USA*

[3] *Department of Mechanical Engineering, The University of Texas at San Antonio, San Antonio, TX 78249, USA*

Abstract

Due to their unpredictable nature, many impact events (e.g., overheight vehicles striking on bridges) go unnoticed or get reported many hours later. However, they can induce structural failures or hidden damage that accelerates the structure's long-term degradation. Therefore, prompt impact detection and localization strategies are essential for early warning of impact events and rapid maintenance of structures. Most existing impact detection strategies are developed for aircraft composite panels utilizing high-rate synchronized measurement from densely deployed sensors. Limited efforts have been made for infrastructure or human habitats which generally require large-scale but low-rate measurement. In particular, due to harsh environments (e.g., deep space habitats under meteoroids), structural impact localization must be robust to limited sensors (e.g., sensor damage during impacts) and multi-source errors (e.g., measurement errors). In this study, an effective impact detection and localization strategy is proposed using a limited number of vibration measurements, especially in harsh environments (e.g. in deep space). Convolutional neural networks are trained for each sensor node and are fused using Bayesian theory to improve the accuracy of impact localization. Special considerations are paid to evaluate the effect of both measurement error and modeling error in the analysis. The proposed strategy is illustrated using 1D structure, and further validated in 3D geodesic dome structure numerically. The results demonstrate that it can detect and localize impact events accurately and robustly on structures.

Keywords: Impact detection, Impact localization, Deep learning, Information fusion, Measurement errors, Modeling errors

1. Introduction

Impacts are hazardous events in which high-velocity objects strike against structures over a short duration. The released high energy may result in structural failures in seconds or induce hidden damage that accelerates the structure's long-term degradation. Two main types of structures are at high risk of impact events: aerospace structures and civil structures. Typical examples for aerospace structures include bird strikes on aircraft and micrometeoroid impact on spacecraft, in which composite panels may produce internal damages without obvious external evidence (aka, Barely Visible Impact Damage[1]). For civil structures, vehicle/ship collisions on bridges are the main threats of concern. The unnoticed collisions may result in another consequential catastrophe for trains/vehicles moving across the bridges (e.g., Big Bayou Canot rail accident[2]). Therefore, prompt impact detection and localization strategies are of great importance for early warning of impact events and rapid maintenance of structures.

Researchers have investigated and developed various techniques regarding the inverse problem of impact detection and localization during the past three decades. These techniques can be generally classified into two categories: physics-based methods and data-driven approaches. The first category relies on the laws of physics. One of the most popular strategies is to utilize the characteristics of impact-induced acoustic waves propagated on the structures. For example, Merlo et al.[3] explored the differences of Time-of-arrival (TOA) of signals and their oscillatory characteristics from a triplet of piezoelectric sensors to triangulate the impact locations. Similarly, Jang et al.[4] estimated the distance between impact and sensor locations using the triangulation method with features obtained from TOA and signal magnitudes from fiber Bragg grating (FBG) sensors. The main challenge of these strategies is that the wave features depend on the property of the propagation medium, especially for anisotropic materials where wave velocities vary in different traveling directions. To address the challenge, one strategy is to obtain a velocity profile for different angles experimentally in which extensive calibration efforts are required [5], or to estimate the profile with an approximate plate theory, which is difficult to derive for complex structures. Alternatively, optimization techniques can help without knowing the prior knowledge of material properties or velocity profiles. For example, Kindu et al.[6] proposed a two-step hybrid technique in which the first step is to obtain the initial estimates of impact location, and the second step is to improve the estimation by minimizing an appropriate objective function using the simplex algorithm. A more detailed discussion about wave-based impact localization can be found in [7]. Another important physics-based strategy is based on the system's model. In this strategy, the impact location is estimated by minimizing a cost function. For example, Li and Lu [8] constructed an inverse model between the unknown force and the measured structural response using the modal superposition method. The impact location is selected from candidate points that minimize the predicted and measured responses by using the Complex Methods. Davis et al. [9] utilized the transfer function of a structure between impact forces at plausible locations and acceleration response. The candidate point that minimizes the standard deviation of force estimates from multiple sensors is considered as impact locations. Yan et al. [10] built state-space models to represent a dynamic system. The inverse analysis is conducted to reconstruct impact time history with Bayesian inference regularization. A nonlinear unscented Kalman filter is used to estimate impact location by minimizing the measured and predicted response errors. Likewise, Saleem & Jo [11] utilized state-space models to estimate the impact location by minimizing the augmented Kalman filter response estimation errors of both acceleration and strain gauge measurements. These model-based methods are generally subjected to the assumption of linear time-invariant systems. In addition, in most cases, the ill-posed problems should be handled carefully by using the regularization technique.

Data-driven methods have increasingly received great attention over the past decade because of their effectiveness for both linear and nonlinear structures. Different from system modeling, it established the relationship between impact locations and response measurements using data interpretation without mechanical information. Shrestha et al. [12] trained a reference database, containing the information of the impact signals from FBG sensors at training grid points. The obtained impact signals from random points are then compared with the reference signals in the database; the impact location is then identified by determining the most similar reference signals and averaging their corresponding impact locations over all the sensors. Hossain et al., [13] proposed a radial basis function network to identify impact locations, using the time-domain peak-to-peak and peak arrival time features from accelerometer measurements as network inputs. It has better performance over conventional Multilayer Perceptron by decreasing the errors of 32.98%. Jang et al. [14] utilized an artificial neural network (ANN) to obtain the relationship between the magnitude of FBG sensors and the distance between impact and sensor locations; the triangulation methods are then applied to identify impact locations, using the estimated distances of impact location from each sensor. Morse et al., [15] also employed the ANN to localize impacts on the composite panels, but applied Bayesian updating and Kalman filter techniques to mitigate the effect of faulty sensor data. The reliability-based impact detection not only improves the accuracy by 20%, but also provides uncertainty quantification in impact location estimations. Tabian [16] developed a metamodel using a convolutional neural network (CNN) for impact detection, localization, and characterization of complex composite structures. The ultrasonic waves from piezoelectric sensors are transferred to 2D images and used as the input for the CNN, whilst the impact locations and categorized energy levels are identified from the CNN output. The data-driven methods generally require large amounts of training datasets for the inversion process.

Most strategies of impact localization discussed above are designed for aerospace structures, identifying impact events on metallic or composite panels. Particularly, the structures are relatively small scale, ranging from small panels with 2 meters in length to the actual aircraft rings with around 10 meters in length. Meanwhile, the local damages or barely invisible damages are more critical to detect in these scenarios, as they are more difficult to identify by inspectors but will threaten the safety of aerospace structures. Accordingly, most strategies utilize high-rate, tightly synchronized data obtained from densely deployed sensors without worrying about sensor limitations. Very few efforts have been conducted for impact detection of civil structures, which are generally large-scale, e.g., bridges can span the distance of tens or thousands of meters. Therefore, the impact detection strategies must be effective and robust using a limited number of sensors to cover a large area. The challenges are much more formidable for civil structures in deep space (i.e., human habitats), where prompt detection of meteoroid impacts is critical. Particularly, the harsh environment in deep space makes sensor malfunctions more likely to occur and the instrumentation/maintenance extremely costly. Most of the current strategies for impact localization are no longer sufficient to handle these challenges.

This paper proposed a novel strategy of impact detection and localization using a limited number of sensors by applying deep learning and information fusion. The proposed strategy works as long as at least one sensor survives in the extreme environment, and the accuracy can be improved if the information is fused from multiple sensors using the Bayesian theory. In addition, considering the harsh environment, special considerations are paid to mitigate measurement errors and modeling errors by exploring data augmentation via adding more sensors. The strategy is illustrated using 1D structure simulation results and further validated in a 3D geodesic dome structure. The results demonstrate that the proposed strategy can accurately identify impact locations under sensor limitations and multi-source errors.

2. Scalable Impact Detection and Localization Strategy

2.1. Research objectives and strategy overview

The objective of this study is to develop a robust and efficient algorithm to enhance the performance of impact detection and localization using multi-sensor measurement, while achieving graceful degradation following individual sensor failures. In particular, it is required to function well for sparsely deployed sensors, and its accuracy is kept relatively high either under measurement errors (i.e., noisy sensor data) or modeling errors (i.e., discrepancies exist between a physical structure and the corresponding numerical model for algorithm development). In addition, as part of the fault detection and diagnosis module for a smart deep space habitat (SmartHab) simulation (MCVT paper), it is also required to be implemented in real-time execution with acceptable computation cost; meanwhile, it should be able to process measurement data at a sampling rate of less than 1 kHz, following the simulation rate of the overall habitat models.

To achieve the objectives, a hierarchical sensor-fusion framework is developed, as illustrated in Fig. 1. It consists of two main stages, as below:

- **Impact detection** is aimed to detect anomalies in the measurement data and then confirm if an impact occurs or not by filtering out irrelevant events. It has two steps: 1) data cleansing is performed continuously to mainly reduce measurement noise by applying wavelet analysis; 2) event detection is triggered only when the sensor data exceeds the user-defined threshold, and it will check the signal envelope and perform curve fitting to detect impacts out of all suspicious events.

- **Impact localization** is designed to localize the impacts, and it is only triggered when the impact detection result is true. It processes the raw measurement data, and performs wavelet transform to extract useful features. These features are then fed into a pre-trained CNN for each sensor node. The obtained probabilities of impact location from each sensor node are then combined and fused by Bayesian theory, which eventually obtains the final impact localization probabilities.

Each step of the above two stages in the flowchart will be presented in the follow-up subsections. Note that in this study, accelerations are considered as sensor readings. But the proposed solution is applicable to other sensor data as well, e.g. strains, as long as they are able to capture structural dynamic responses.

2.2. Impact detection: data cleansing

The purpose of data cleansing in this strategy is to facilitate threshold-based event-driven data processing. Particularly, the strategy is implemented to be triggered, if the measurement data exceeds the user-defined threshold. But a certain level of noise in measurement data will confuse the triggering conditions. If the threshold is defined conservatively low,

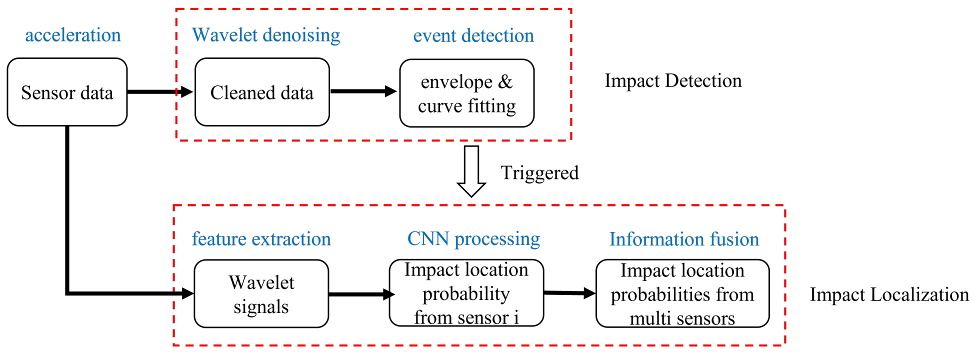

Figure 1: Flowchart of the proposed solution

the strategy will be triggered many unnecessary times, consuming lots of computational resources; otherwise, it may miss the impact events, or at least a portion of event data. as illustrated in Fig. 2. Therefore, a fast and effective strategy is highly desired to preprocess the data for impact detection analysis. It is worthwhile to mention that, data cleansing is only applied for impact detection, aimed at finding the right starting time of impact responses. The impact localization leverages the obtained information about impact starting time, but still uses the raw data for the subsequent analysis, such that it will not lose any useful information.

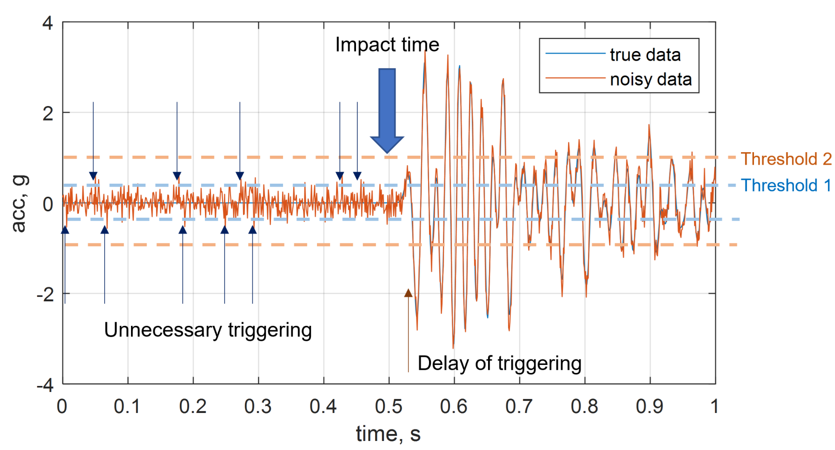

Figure 2: Illustration of faulty triggering in noisy data

There are many noise reduction strategies available for online data processing. A common strategy is using low-pass filters, considering that noise power is generally concentrated in the high-frequency domain. In this strategy, it is assumed that the structural response is mainly in the low-frequency domain, which is not affected by low-pass filtering. It is true for most common structures in which the highest natural frequency of interest is smaller than the Nyquist frequency of sensor data acquisition, but it no longer holds for high-stiffness structures with a relatively low-rate measurement where their Fourier spectra and noise power overlap. Another popular strategy recently is to apply machine learning algorithms, e.g., autoencoder or principal component analysis, however, they are relatively complex and more suitable for image noise reduction. In this study, following the study [17], a discrete wavelet transform (DWT) is applied for noise reduction, which is fast and effective.

The DWT decomposes a given signal $x(t)$ into a series of discrete scales, each of which represents a certain frequency band. At each frequency band, the DWT can obtain a set of coefficients describing the time evolution of the signal. The DWT expansion of $x(t)$ can be presented as below,

$$x(t) = \sum_j \sum_k \gamma_{j,k} \Psi_{j,k}(t) \tag{1}$$

where,$\gamma_{j,k}$ is the coefficient of wavelet expansion at scale j and location k. $\Psi_{j,k}(t)$ is the discretely sampled mother wavelet, and $*$ represents complex conjugate transpose.

$$\gamma_{j,k} =< x(t), \Psi_{j,k}(t) >= \int x(t) \Psi^*_{j,k}(t) dt \tag{2}$$

$$\Psi_{j,k}(t) = 2^{-j/2} \Psi(2^{-j}t - k) \tag{3}$$

There are a number of wavelet functions to choose, and choosing the right function usually depends on the similarity or correlation between the wavelet and the given signal. Here, we follow the paper [17] to choose Daubechies wavelets of order 4 (db4).

After selecting the mother wavelet and number of decomposition levels N, we can complete the decomposition of the measurement data. The next step for denoising is to perform thresholding of coefficients in the wavelet domain. The underlying assumption is that, the wavelet decomposition can concentrate the signal into several certain large coefficients, while the noise corresponds to the relatively small value but large number of counterparts. By determining the threshold for each level of wavelet decomposition, we can identify and shrink the coefficients below the threshold that are related to noise. Afterward, the inverse wavelet transform is conducted to reconstruct the signal with adjusted coefficients, eventually achieving the clean signal $x(t)_c$. In this study, the MATLAB built-in function, *wdenoise*, is leveraged to realize data cleansing with wavelet transform.

2.3. Impact detection: curve fitting

The objective is to reduce impact detection errors in event-driven monitoring in two aspects: (i) eliminating false negative rates, i.e., no missing impact events; (ii) minimizing false positive rates, the high value of which may unnecessarily upset engineers or result in the lost of trust for the monitoring systems. To achieve this objective, a general idea is to set the threshold to be reasonable, so that no significant events will be missed and minimal events of no interest are recorded. Typical examples of events of no interest in this study include anomaly readings like drifts, ambient vibrations, and other large disruptions like ground motions and strong winds. Fig. 3 shows several false detection scenarios for illustration.

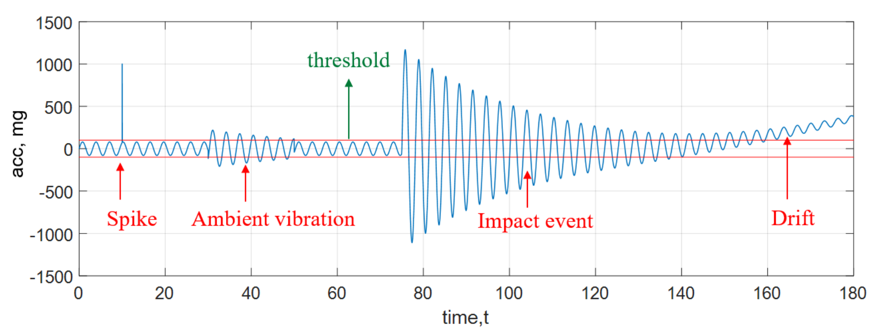

Figure 3: Illustration of false detection scenarios in a data-centric view

In this study, we only focus on a single event of interest, i.e., impacts. Therefore, we can directly classify the captured events as impacts and other events. The proposed strategy herein is to leverage physics and domain knowledge of impacts. The impacts can generate an acceleration record in which the amplitude decays exponentially. To extract this unique feature, a Hilbert transform is performed for each acceleration record $x(t)$ to obtain the signal envelope. The Hilbert transform can be used to obtain the analytic representation of a signal in the form of a complex-valued function with no negative frequency components. In the analytic representation $a(t)$, the real part is the signal itself $x(t)$, and the imaginary part is the actual Hilbert transform $h(t)$. The envelope of the signal $e(t)$ can then be obtained by calculating the magnitude of $a(t)$, as expressed below.

$$H(x(t)) = h(t) = \frac{1}{\pi}\int_{-\infty}^{\infty} \frac{x(\tau)}{t-\tau} d\tau \tag{4}$$

$$e(t) = |a(t)| = |x(t) + ih(t))| = \sqrt{x(t)^2 + h(t)^2} \tag{5}$$

Afterwards, we can curve fitting the signal envelope $e(t)$ using the following equation, assuming that the signal of events decays exponentially.

$$e(t) \approx me^{-nt} \tag{6}$$

The obtained (m, n) is the index to describe the decay of signal amplitude. By comparing n with a user-defined value, we can tell if the signal is related to impact events or not. By principle, n should be reasonably large. In the end, we can classify the detected events into impact events and other events.

Alternatively, these significant events can be viewed as anomalies of measurement data in a data-centric view, and machine learning methods can help to further classify them accurately, including but not limited to impacts, ground motions, spikes, and drift. However, it requires a comprehensive list of possible significant events or anomalies and needs corresponding accurate datasets from the targeted structure to train the machine learning models. Therefore, it is not considered in this study.

2.4. Impact localization: feature extraction and CNN processing

The objective is to estimate impact locations using data-driven methods. The time-invariant features of impact responses are utilized, and hence CNNs are adopted here. Instead of giving exact coordinates, we divide the surface areas of structures into multiple zones and apply the CNN to classify which area is most likely subjected to impacts. This is actually following the requirements of fault detection and diagnosis for the SmartHab (MCVT paper), in which probabilities of each zone subjected to impacts should be provided.

Fig. 4 shows the framework of the proposed data-driven strategy for impact localization. After impact detection is triggered and successfully achieved, a certain length of time history record starting from the triggering time is collected. For the measurement datasets from each sensor, a CNN classifier is trained to provide probabilities of every zone of the structural surface. If we deploy M sensors, M classifiers will be obtained, which share the same CNN architecture but different weight values. In contrast to many similar studies, instead of fusing information from multiple sensors before feeding into data-driven methods, we conduct a fusion of information after impact localization results from each classifier are obtained. This idea makes the proposed strategy robust and scalable. If some sensors are damaged after impact events, the measurement data from the survived sensors can still present acceptable results of impact localization. In other words, the proposed strategy functions well as long as one sensor survives. The more sensors survive, the higher the accuracy it can achieve. The feature extraction and CNN architectures will be discussed in the following paragraphs, while the information fusion part will be presented in Section 2.5.

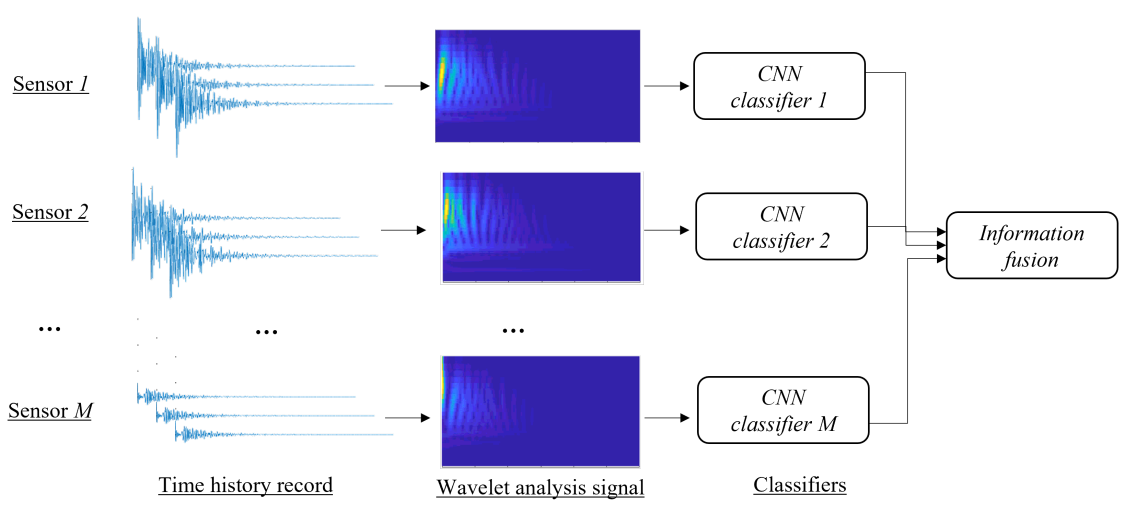

Figure 4: A scalable data-driven framework for impact localization

The time-frequency energy distribution is also leveraged here for feature extraction. Instead of using spectrograms via the short-time Fourier transform in conventional studies, we use continuous wavelet transform to get more informative features for the CNN. In particular, the wavelet transform uses windows that are longer for lower frequencies and shorter for higher frequencies, which is superior to spectrograms which employs the fixed window for all the frequency band. Such multi-resolution analysis of the wavelet transform provides a sharp time-frequency representation, ideal for analyzing nonstationary signals containing the information of impact occurrences. The continuous wavelet transform of a signal $x(t)$ is expressed below,

$$W_{\psi}^{x}(a,b) = |a|^{-1/2} \int_{-\infty}^{\infty} x(t)\psi(\frac{t-b}{a})dt \tag{7}$$

where a is the scaling factor, b is the translating factor, and ψ is the mother wavelet function. In this study, the MATLAB built-in function, *cwt*, is leveraged to realize continuous wavelet transform, and the analytic Morse wavelet is adopted in this function. The resulting signal is a 2D matrix where each row corresponds to one scale a_i. The column size of the signal is equal to the length of the original time history data $x(t)$. The total size of the input is 61 (scale levels) x 501 (sample number), given that the signal is sampled at 1000 Hz.

Fig. 5 shows the architecture of the CNN for Sensor i for impact localization. It reads 2D image signal from wavelet transformation, and extracts shift-invariant features through k feature learning layers. The feature learning layer sets include a convolutional layer, a batch normalization layer, an activation layer, and a max pooling layer. The number of feature learning layers is determined by the complexity of the problem. Specifically, if the structure for impact detection is soft with a low damping ratio, its time-frequency representation is relatively simple, and $k = 3$ is sufficient. But for high-stiffness structures, k should be larger. More discussions can be found in Section 3. In addition, the number of neurons in the fully connected layer, l, is determined by the number of zones for impact locations.

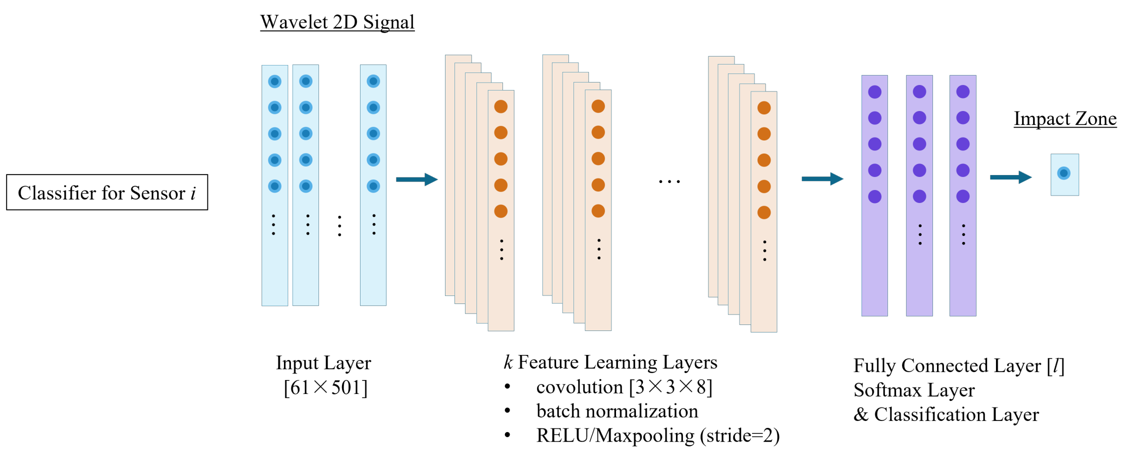

Figure 5: Architecture of a convolutional neural network for Sensor i for impact localization

2.5. Impact localization: information fusion

The objective of information fusion is to combine the probability outputs from CNN classifiers for each sensor, and produce more accurate results for impact localization. To this end, Bayesian theory is adopted here. Particularly, the probability of an impact $I_{r,s}$ is defined as below,

$$I_{r,s} = p(L = r|S_i = s) = f_i(s) \tag{8}$$

where f_i is the probability outputs from CNN classifier i corresponding to Sensor i; r is one of the potential zones on the structural surface, and s is the wavelet signal observed by Sensor i. Furthermore, the probability of an impact J_r inferred by M sensors can be expressed as below,

$$J_r = p(L = r|S_1 = s_1, S_2 = s_2, ..., S_m = s_m) = \frac{\prod_{i=1}^{M} I_{r,s}}{\sum_u \prod_{i=1}^{M} I_{u,s}} \tag{9}$$

In addition, a loss function ℓ is defined to identify the most likely impact location in which the loss function is minimized. The optimal localization results, J^* is expressed below,

$$J^* = arg \min_h \sum_n \ell(h, r) J_r \tag{10}$$

where r is the true impact location, while h is the searched impact location. The loss function ℓ can be defined as a square matrix, where the diagonal items are all zeros, and the rest of them are ones. Its dimension is $U \times U$, where U is the number of potential impact zones.

$$\ell = \begin{pmatrix} 0 & 1 & \cdots & 1 \\ 1 & \ddots & 1 & \vdots \\ \vdots & 1 & \ddots & 1 \\ 1 & \cdots & 1 & 0 \end{pmatrix} \tag{11}$$

In Eq. 9, additional modification is made to scale the probability outputs from each classifier $I_{r,s}$, such that, we do not take $I_{r,s}$ from each sensor with equal confidence during information fusion. Here, in a set of survived sensors, if sensor readings in Sensor p are much smaller than that in Sensor q, we consider that I_{r,s_p} is less reliable than I_{r,s_q}, assuming the information obtained from the low magnitude of sensor readings are contaminated by noises. The modified probability output I^{+}_{r,s_i} is scaled by the ratio of root mean square among each obtained measurement dataset, defined as below,

$$I^{+}_{r,s_i} = I_{r,s_i}^{(rms_i/rms_{max})^w} \tag{12}$$

where w is the index that can be adjusted by users; the larger w means more significant scaling. In the end, softmax normalization should be performed to I^{+}_{r,s_i}, ensuring that the sum of probability for each impact location from Sensor i is one. In the extreme case, if the sensor reading from Sensor i is almost zero, its output probability is very close to $1/U$ for each location, where U is the total number of potential impact locations.

3. Illustrative Examples

This section presents a numerical illustration of the proposed strategy by building a 1-dimensional (1D) model and discussing the performance of both impact detection and impact localization. The proposed strategy is written in MATLAB language and trained/tested using the Deep Learning toolbox.

3.1. 1D model description

A 1D numerical model is established to illustrate the capability of the proposed strategy, as shown in Fig. 6. It is a 10-degree-of-freedom (DOF) linear system. The governing motion of the equation is expressed as,

$$M\ddot{\mathbf{x}}(t) + C\dot{\mathbf{x}}(t) + K\mathbf{x}(t) = \mathbf{f}(t) \tag{13}$$

For simplicity, the mass, stiffness and damping parameters for each DOF are set to be the same. Specifically, $m_i = 29.13kg$, $k_i = 1190 \times 10^3 N/m$, and modal damping ratio is considered here, with damping ratio $\zeta_i = 0.0097$.

$$C = \Phi^{-T} diag(2\zeta_i \omega_i m_i)\Phi^T \tag{14}$$

where Φ is the modal matrix, and ω_i is the natural frequency for i^{th} mode. The values of these parameters are referred to the experimental setup parameters in the paper [18]. Its natural frequencies are shown in Fig. 7.

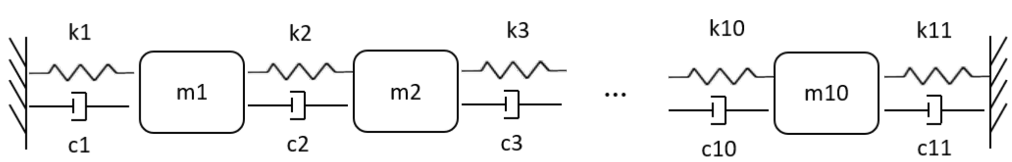

Figure 6: 1D model with 10 degree-of-freedoms

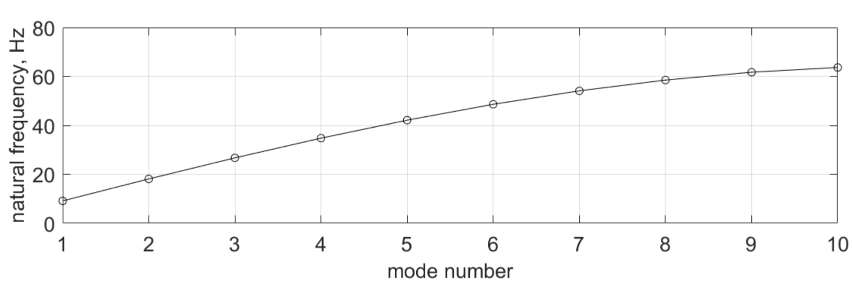

Figure 7: Natural frequencies of 1D structural model

The 1D model is implemented in Simulink. The structural dynamic responses, i.e., accelerations of all DOFs, are obtained with a sampling rate of 1000 Hz and a time history of 10 s. The impact force is simulated as an impulse signal with a duration of dt. It is applied to any one of DOFs at 2 s, with different levels of amplitude, ranging from 0.1 kN to 10 kN. In addition to ideal measurement data, Gaussian white noise with zero mean and unit variance is also added to some simulation results. In particular, different levels of noise floors in dBm are considered to illustrate the performance of the proposed strategy in various structural operating environments. Furthermore, modelling errors are included for some simulations, to emulate the discrepancies between the ideal structural model for the CNN training and the actual physical structure with uncertainties. The definition of modelling error Err is defined as the summation of discrepancies for all stiffness k_i.

$$\begin{aligned} k_i^* &= k_i + \Delta k_i^+, \Delta k_i^+ \in [-0.1, 0.1] \\ Err &= \sum_i |\Delta k_i^+| = 2\%, 5\%, 10\%... \end{aligned} \tag{15}$$

3.2. Impact detection

Fig. 8a shows the comparison between noisy data and clean data after wavelet transforms for the illustration of data cleansing in impact detection. An impact force of $1kN$ is added to the first node (1^{st} DOF), and the acceleration at the last node (10^{th} DOF) is recorded. In the meantime, white Gaussian noise is added, with a signal-to-noise ratio (SNR) of 2. After applying the wavelet transform, the noisy signal before impact is cleaned, and the SNR is increased to 13. A more systematic investigation is carried out to record the change of SNR after data cleansing using the wavelet transform, as shown in Fig. 8b. The wavelet denoising can help to increase the SNR of raw signals by around 10 in this example.

To further demonstrate the benefit of data cleansing, the impact force is added to each of 10 DOFs at $2s$ and the acceleration record of over $10s$ from the 10^{th} node is collected. To make it representative, for each node, 100 times of impact forces with the magnitude of a random value from $0.1kN$ to $1kN$. In sum, a total number of 1000 data sets are obtained, and each data set adds the white Gaussian noise with an SNR of 10. Assuming the trigger condition is $0.1g$, the triggering time when the acceleration record exceeds the threshold is collected and compared to the ground truth of $2s$. For the noisy data, the triggering time is mostly located before $2s$, because the noisy signal confuses the triggering conditions; after data cleansing, most data sets have the correct triggering time for impact events, minimizing unnecessary triggering. The accuracy of the correct triggering time is recorded for each level of SNR from 1 to 30. The summary of results is compared in Fig. 9a. Also, for illustration of the effect of impact threshold, $0.1g$ and $0.5g$ are both considered, showing that increasing the threshold can help to achieve higher accuracy of triggering time against the noise effects. To systematically analyze the effect of triggering threshold, similar analysis is conducted for different levels of threshold values from 0.01 to 0.1, as shown in Fig. 9b.

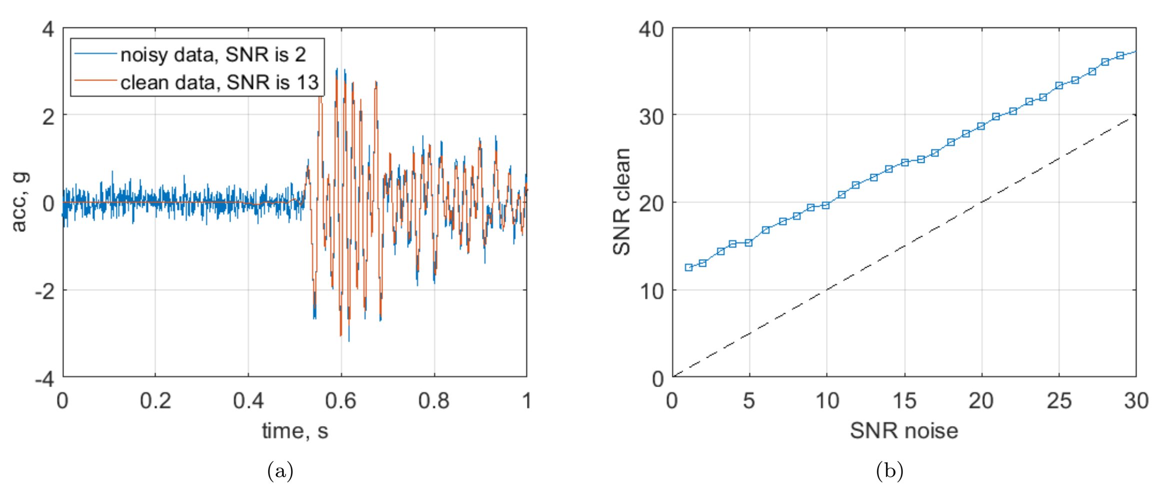

Figure 8: Noise reduction using wavelet transform: (a) illustration, and (b) SNR summary

With appropriate triggering time, the impact event detection is demonstrated using the domain knowledge, as shown in Fig. 10. The acceleration record is truncated after triggering and the total length of $5s$ is analyzed, for each of the 1000 data sets collected before. Their envelopes are first calculated and then curve-fitting of exponential functions is conducted to obtain the parameter, n. The value of n is finally summarized in the histogram; most value is around 3. As an illustrative example, curve-fitting of an impact response is carried out, and the value n is 2.98, as shown in Fig. 10b.

3.3. Impact localization

After an impact is detected, the proposed strategy is then designed to localize this significant event. Note that, the previous step of impact detection provides the triggering time at which the raw time history data starts to record. As an illustration, Fig. 11 shows the

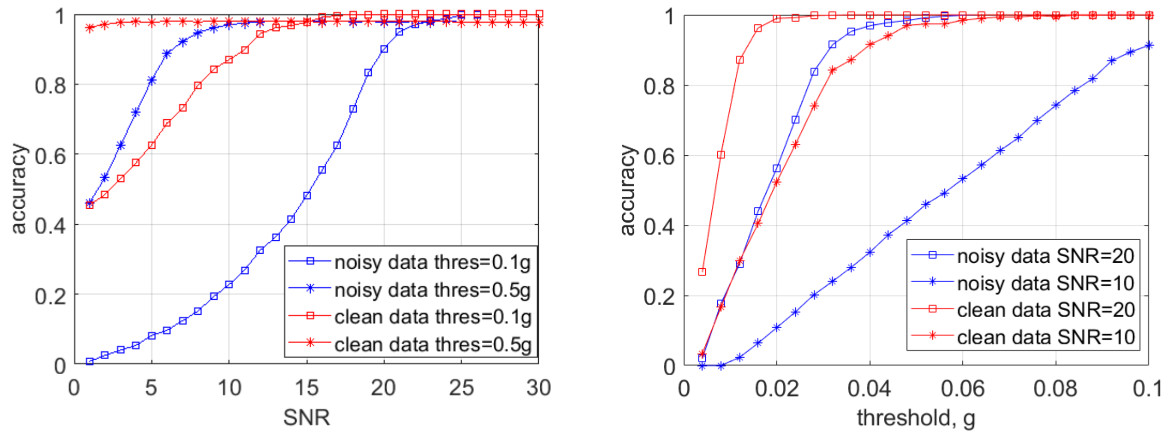

(a) (b)

Figure 9: Threshold-based triggering time: (a) accuracy under different SNR, and (b) accuracy under different threshold

.

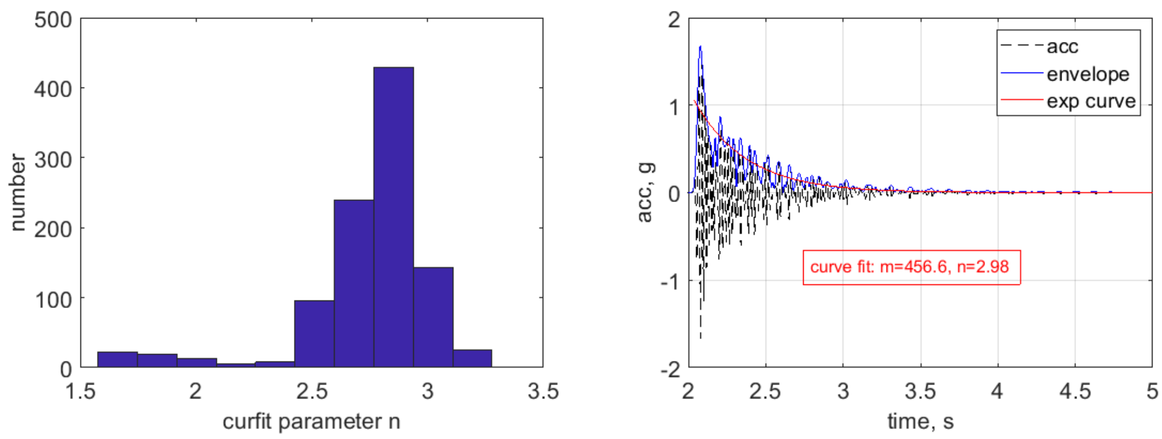

(a) (b)

Figure 10: Impact event detection using curve fitting: (a) exponential function parameter, n; (b) illustrative example

feature generation for the inputs of a CNN model. The architecture of the CNN model follows that in Fig. **??**, in which the number of feature learning layers is 3, the filter size is 3 by 3, and the number of filters is 3 per layer. Particularly, the impact occurs at 1 second on the 1ŝt DOF, with the amplitude of $1kN$. The data collected on the 2^{nd} DOF is plotted in the figure. The obtained wavelet transform signal of raw time history data contains essential information starting from the impact. As shown in Fig. 11a, the impact time history signal gradually decays to a negligible value, within 2 seconds after the impact occurs. In addition, referred to Fig. 11b, the most information (bright area) is located between 15 Hz and 115 Hz. Therefore, only 2 seconds of signal within a frequency band of 15 to 115 Hz is processed for wavelet transform to allow higher resolution of input features for the CNN of impact localization. Such wavelet transforming process is carried out for all the 1000 data sets which are defined in Section 3.2. The outputs are the locations of impact forces, executed on each DOF in the 1D model, with the value ranging from 1 to 10. Within the entire data set, 60% of the is the training subset, 20% is the validation subset, while the rest 20% is the testing subset.

The learning rate is set to be 0.001, and the batch size is defined to be 100. Fig. 12a shows the learning curve for the sensor located on Node 10. As can be seen, both training and validation rates quickly converge to 100% for accuracy. 25 iterations are sufficient to achieve the best results. Fig. 12b shows the confusion matrix, where all the impact locations are successfully identified with no errors. The same behavior is found for the sensors located in other nodes. Therefore, there is no need to do additional information fusion, as a single sensor is sufficient to achieve 100% accuracy. In addition, the trained CNN classifiers are further tested with data corrupted with measurement noises without information fusion. It is found that, even for the data with the signal-to-noise ratio of 10, the accuracy of impact localization can be achieved with 99.9% or so. This is because the 1D structure is relatively simple to construct the relationship between the impact location and the measurement data. In the

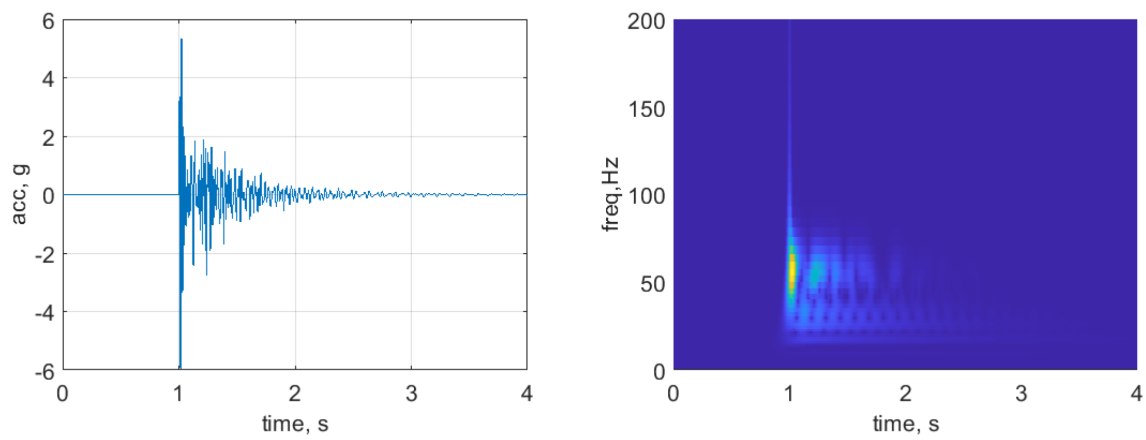

(a) (b)

Figure 11: Illustration of feature inputs for deep learning: (a) time history record, and (b) wavelet transform results

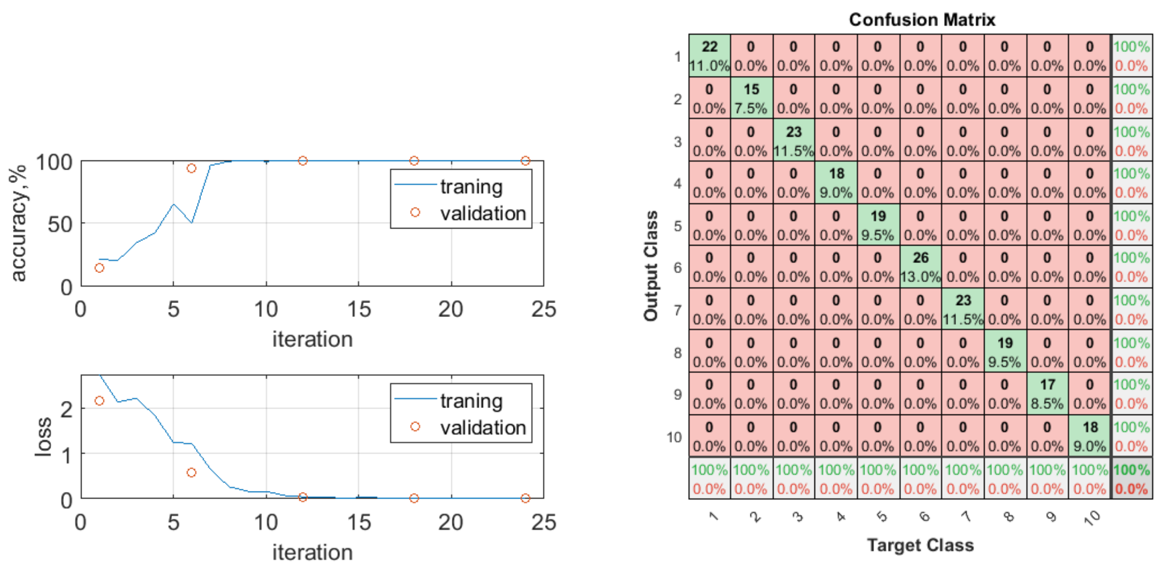

(a) (b)

Figure 12: Impact localization for 1D structure: (a) learning curve, and (b) confusion matrix

following sections, more realistic considerations are applied to evaluate the performance of the proposed strategy.

3.4. Discussion on high-stiffness structures and measurement errors

To consider more realistic situations, the structural model is modified. Particularly, in real applications, the structural system has high stiffness (e.g., dome-like structure in most deep space habitat designs) but a limited sampling rate for measurement. In this case, the collected measurement data can only cover a very limited frequency band of interest and hence limited useful information. Such a situation eventually increases the difficulty of successful impact localization. In this section, the stiffness of the 1D structure is increased, by multiplying the k_i with a factor of 350. As a result, its natural frequencies are increased, as shown in Fig. 13. If the sampling rate is kept the same as 1 kHz, the effective frequency band can only cover the first three natural frequencies. Following the same setup of impact force in Fig. 11, the acceleration time history record is collected at the same node. As can be seen in Fig. 14a, compared to the low-stiffness 1D structure, the captured amplitude in the time domain is reduced. This is because the power of the signal is now concentrated in the higher frequency band that is not able to be captured using the same sampling rate. Meanwhile, the signal decays in a much quicker way than in the previous case. The wavelet transform results of corresponding raw time history data are shown in Fig. 14b, where the most informative area is also reduced and three spots corresponding to the first three modes can also be clearly seen.

Based on what we observed, only 0.5 seconds of signal within a frequency band of 100 to 500 Hz is processed for wavelet transform analysis, and the obtained spatial-temporal information is used as the input for the CNN. The CNN architecture for impact localization

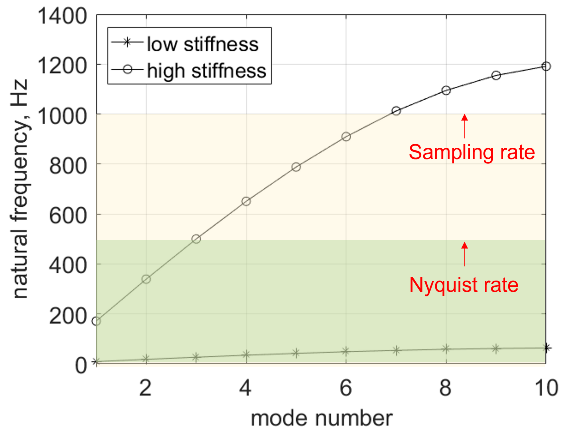

Figure 13: Natural frequencies of low-stiffness and high-stiffness 1D models

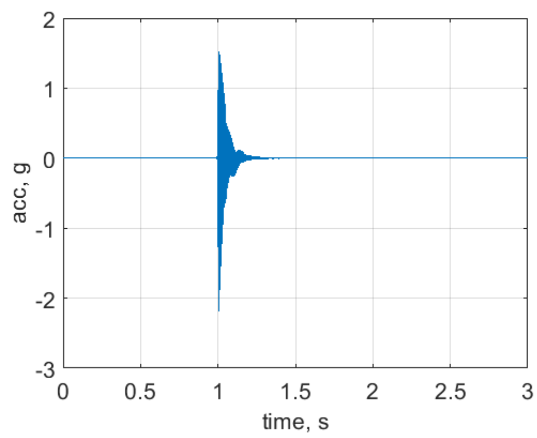

(a)

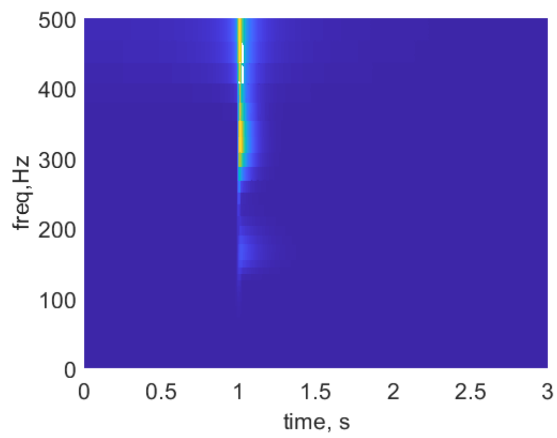

(b)

Figure 14: Illustration of feature inputs for stiff 1D structure: (a) time history record, and (b) wavelet transform results

is kept to be the same as that for the low-stiffness 1D structure. The same procedure is repeated to build the response database for the high-stiffness 1D structure, where a total number of 1000 raw acceleration records are collected. These data records are then divided into three parts randomly for training, validation, and testing, respectively. In addition, the learning rate and batch size are also the same as that in Section 3.3. Compared to the low-stiffness 1D structure, the learning curve of the CNN for the high-stiffness 1D structure now needs longer iterations to converge to a reasonable accuracy. In addition, the overall accuracy of the CNN is reduced. The same process is conducted by using a single sensor in each node of the 10-DOF model. In addition, to consider uncertainties of learning accuracy, for each sensor location, learning and testing are repeated 10 times with randomly divided data sets. The summary of test accuracy is plotted in Fig. 15a. As can be seen, each sensor location can achieve a reasonable accuracy of above 95%, with a small variation of accuracy among different locations.

Based on that, information fusion is then applied to examine the localization accuracy change, as the number of available sensor nodes increases on the 10-DOF stiff structure. Without loss of generality, we choose the sensor on the 1^{st} node as a single sensor to detect impact location, and then gradually add more sensors to conduct information fusion for impact localization, including 3^{rd} node, 5^{th} node, 7^{th} node, and 10^{th} node, which are labelled as S1, S3, ..., S10. During the test, different levels of Gaussian white noise are added to the data sets to emulate measurement errors, controlling the noise energy from $-90dBm$ to $-60dBm$. The impact location classifier for each sensor is trained using the data set with the noise floor of $-90dBm$, and the same classifier is used to test the data sets with higher levels of noise energy. The results are summarized in Fig. 15b. As can be seen, when the noise is $-90dBm$, impact localization based on only S1 has satisfactory accuracy. Adding S3 can help to increase the precision to almost 100%. Afterwards, adding more sensors, however, can only result in a small increase in accuracy, meaning that two sensors are sufficient to obtain the best impact localization. When the noise energy increases, the accuracy of impact localization for the same sensor setup decreases, but information fusion helps to maintain the high accuracy by adding more sensors, mitigating the adverse impact of noise errors. On

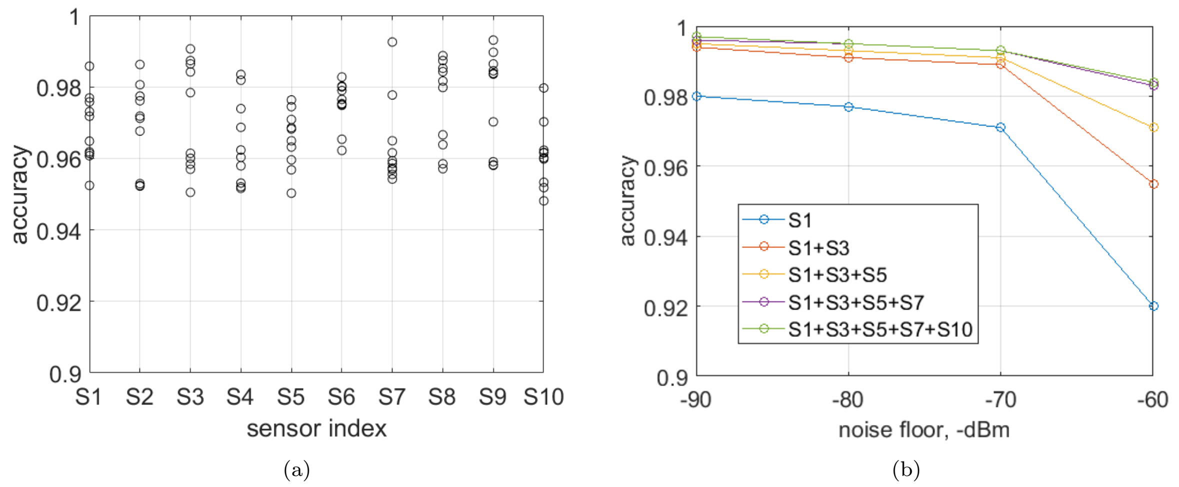

Figure 15: Impact localization for 1D stiff structure: (a) accuracy for different sensor locations, and (b) information fusion results against noise floor

the other hand, such analysis can also help engineers to optimize the sensor deployment for their specific purpose, by adding or removing sensors.

3.5. Discussion on modelling errors

Another important aspect of realistic problems is the modelling error. As described in Section 3.1, modelling error is introduced to the original 1D structure, with different levels of severity, ranging from 5% to 20%. For each degree of freedom, the stiffness change has a negative or positive sign randomly, meaning that it can either increase or decrease. The model without errors is adopted to generate response data and train the CNN classifier for impact localization. The models with random errors, representing real structures, are then used to generate measurement responses for testing. The objective is to evaluate the robustness of the proposed strategy against modelling errors. The modelling error is first added to the 1D soft structure, and the pre-trained classifier for sensors on each node is tested afterwards. The test results show that all the classifiers achieve almost 100% accuracy even with large modelling errors of up to 20%. Fig. 16a shows the test result of the sensor on Node 10, for the classification of impact locations with the modelling error of 20%. It demonstrates that the proposed strategy works well even with large modelling errors for the 1D soft structure. The same process is conducted to test the accuracy of the classifier for impact localization for the 1D stiff structure. The results are summarized in Fig. 16b. Similar to the findings in Section 3.4, impact localization is more challenging for high-stiffness structures, where accuracy drops significantly by over 10%, when the modelling error increases to 20%. Again, the information fusion helps to mitigate the adverse impact of modelling error; but adding more sensors does not help a lot herein. Therefore, effective strategies are desired to improve the performance of the proposed strategy against modelling errors.

Alternatively, the modelling error is considered as a specific type of over-fitting problem in machine learning. In particular, the 1D numerical model without error generates an ideal training data set, and the CNN classifier fits exactly against this data set. The ideal numerical model is different from the real structure with some certain errors. The measurement data from the real structure can be considered as testing data, and the difference between testing data sets from the real structure and the numerical model is the ”noise” that the CNN classifier is overfitted. In other words, after the learning accuracy surpasses a certain point, the better the CNN classifier fits the ideal numerical model, the worse it predicts the real structure. Therefore, effective strategies adopted in machine learning to mitigate overfitting are considered in this study. The strategies include, (i) dropout, meaning that we randomly drop units from the neural network, (ii) regularization, meaning that we shrink the coefficient estimates towards zero, and (iii) data augmentation, meaning that we expand the training data sets by adding certain amounts of additional data (this data comes from the model with artificially generated errors).

To evaluate and compare the effect of different strategies, the CNN classifier for the sensor on the 10^{th} Node is retrained and compared. The original classifier obtained for impact localization served as the reference for comparison. The dropout of 20% units is first considered by adding the *droplayer* in MATLAB. As shown in Fig. 17a, the results show that the accuracy is decreased without introducing the modelling error, but the accuracy

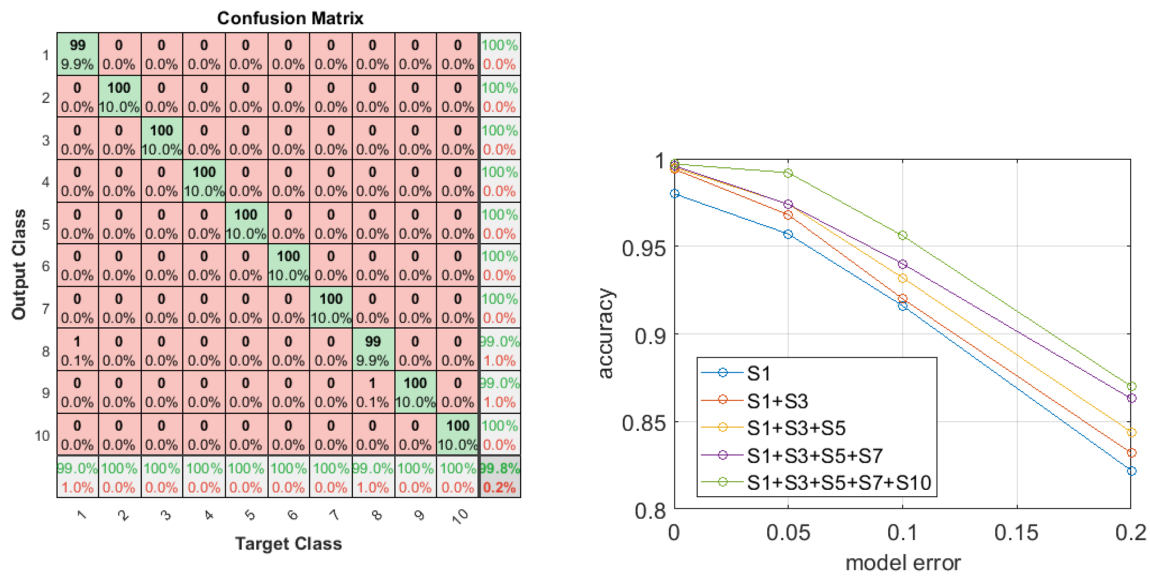

(a) (b)

Figure 16: Modelling error for 1D structure: (a) accuracy for soft structure using single sensor under 20% error, and (b) accuracy for stiff structure using multiple sensors

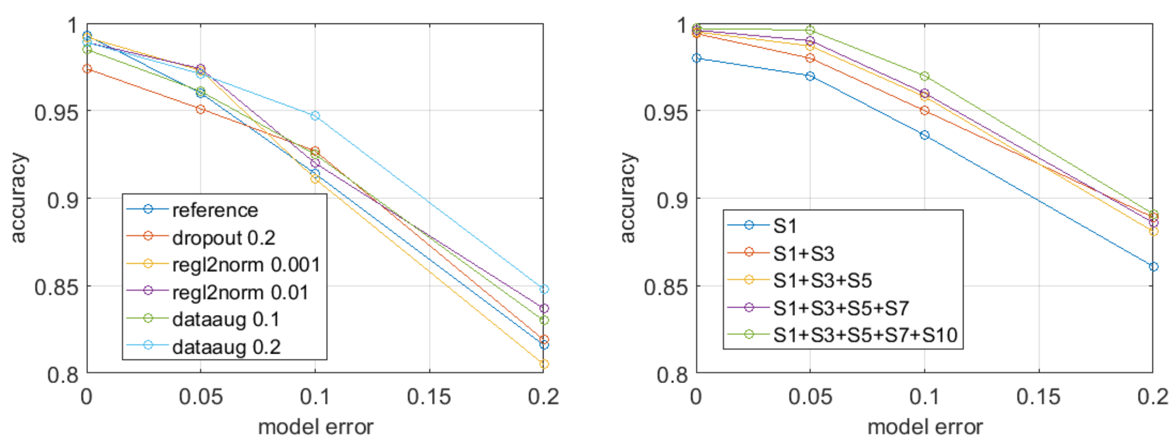

(a) (b)

Figure 17: Modelling error mitigation for 1D stiff structure: (a) accuracy comparison between different strategies, and (b) accuracy using data augmentation and information fusion

is slightly increased for the cases with larger modelling errors. The performance is not improved, when the dropout ratio is increased. For regularization, the most common way, L_2 norm, is considered, by adding a penalty for weight size to the loss function. The first value of L_2 is set to be 0.001. The accuracy is increased for small modelling errors compared to the reference value, but it is decreased for large modelling errors. The increase of L_2 can contribute to better performance against modelling error. For data augmentation, additional data sets are generated using a model with artificially inserting errors. Particularly, for each data set, the stiffness of each DOF in the model is increased/decreased by a random value of less than 0.02. Here, we control the number of data sets added to the original data sets. In the test, 10% and 20% of the total number of original data sets are added for the additional data sets, respectively. As can be seen, the increase of data augmentation can help to increase the accuracy, especially for large modelling errors, and 20% data augmentation outperforms all the other strategies.

In the follow-up test, 50% data augmentation is considered to retrain the CNN classifier for each of the five nodes, and their information fusion results are shown in Fig. 17b. As can be seen, the accuracy of the proposed strategy increases either using a single node or using multiple nodes, compared to the results shown in Fig. 16b. It demonstrates that the idea of using data augmentation can significantly mitigate the modelling error effects.

4. 3D Geodesic Dome Numerical Application

This section presents the application of the proposed impact detection and localization strategy on a 3D geodesic dome. This type of dome structure is widely recognized as suitable for deep-space habitats in the future city. The meteoroid impact is one of common and

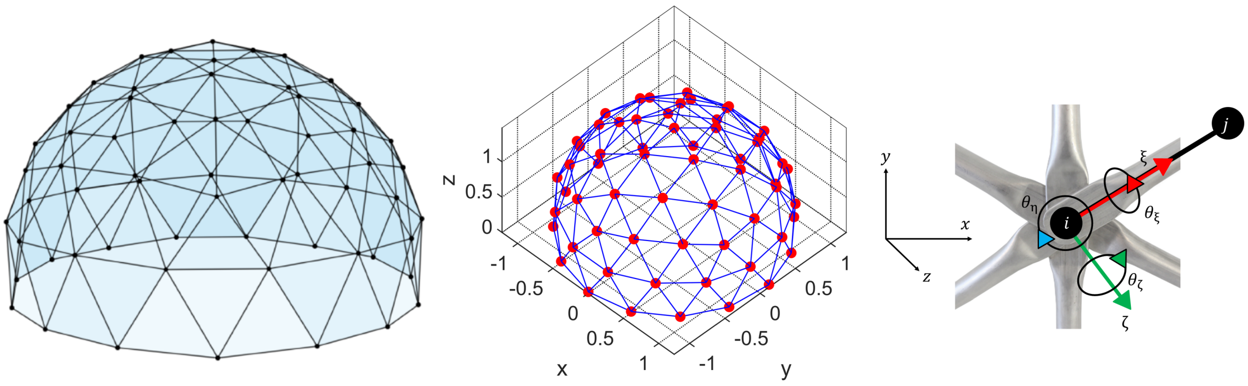

Numerical model overview — Model coordinates — Joint schematics

Figure 18: 3D Geodesic Dome Structure

disastrous hazards to the deep space habitat. Therefore, the objective of this application is to rapidly and accurately detect and localize such critical events.

4.1. Finite element model and impact simulation

A 3D finite element model is built in MATLAB to emulate the behavior of geodesic dome structures, with a height of 1.5 m and a diameter of 2.5 m. It has 61 joints and 165 members, which form the skeleton of the dome-like structure, as shown in Fig. 18. Each member is considered a beam element that can carry both axial and bending loading; each joint is illustrated in the figure, connecting up to 6 members. A member (marked in black) constitutes two nodes (i.e., i and j). Its stiffness matrix is then computed as,

$$[k_{e-unity}] = (E_T[k_{eT-unity}] + E_B[k_{eB-unity}]) \tag{16}$$

where, E_T and E_B are the modulus of elasticity for axial and transverse loading, respectively. $[k_{eT-unity}]$ is the stiffness matrix accounting only for the axial loading, whereas $[k_{eB-unity}]$ for transverse loading. Similarly, considering ρ as the density of the material at the dome, the mass matrix can be defined as, $[m_e] = \rho[M_{e-unity}]$. The global stiffness and mass matrices are then assembled from 165 struts, by considering appropriate transformation matrices $[T_e]$ for each member. Table. 1 summarizes the values of variables in this model. Rayleigh damping is employed for the following dynamic analysis.

Table 1: Variables in the numerical model

Variables	Values	Units
Modulus of elasticity (bending)	22.95	GPa
Modulus of elasticity (axial loading)	63.16	GPa
Density of steel	13950	kg/m^3
Cross section area of members	0.0018	m^2

An impact force is applied to a predetermined joint, perpendicular to the surface of the dome structure. Applying the Newmark-Beta algorithm, structural dynamic responses are obtained, at the sampling rate of 1000 Hz and a duration of 5 seconds. Accelerations of several pre-selected joints are collected in the direction of surface normal, mimicking the usage of uniaxial accelerometers attached to the dome. To illustrate the impact responses of the dome-like structure, a force of 10 kN is applied to the top of the dome vertically. The time history responses of accelerations in several joints are recorded in Fig. 19. The responses attenuate quickly within 0.3 seconds, indicating its high-stiffness features. Accordingly, if using a sampling rate of 1000Hz, very limited information can be captured within the effective band of 0-500Hz, as demonstrated in the frequency domain plot in Fig. 19.

The dome surface is divided into 11 zones. As shown in Fig. 20, six joints on the top are combined as the first zone, highlighted in red; four joints are combined as a new zone, for the remaining joints, highlighted in different colors. Accordingly, the impact localization is then formulated as a classification problem, identifying the zone index out of 11 zones. Furthermore, a total number of 11 uniaxial accelerometers are deployed on the surface of the structure, as indexed and shown in Fig. 21. There are one sensor on the top, five sensors

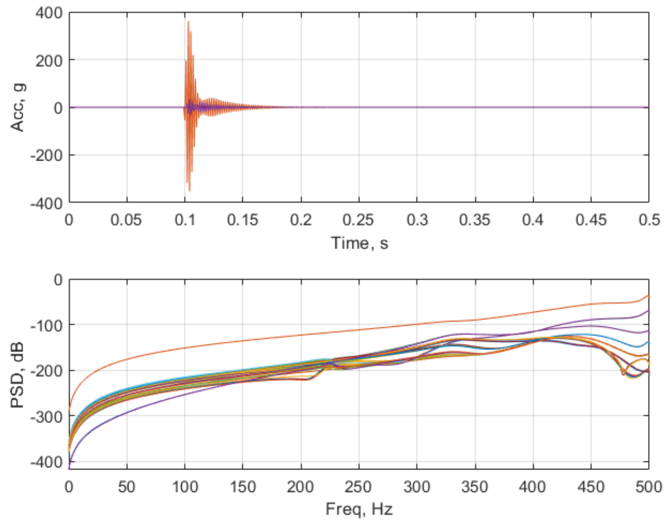

Figure 19: Impact simulation response data

on the middle level, and five sensors on the lower level. The orientation direction of the accelerometers is perpendicular to the surface of the dome structure.

To facilitate evaluation and ML model training in the following sections, extensive simulations are conducted with various impact locations and impact intensities. In particular, we conduct simulations at each of the 46 joints (excluding the bottom layer joints that have ultra-low possibilities of meteoroid impacts) and at different magnitudes of impact forces (i.e., 100 force levels ranging from $0.1kN$ to $10kN$). In total, we obtained 4600 sets of impact simulations and collected 11 acceleration records for each simulation. Furthermore, each record is polluted with different levels of Gaussian white noise to evaluate the robustness of the proposed strategy.

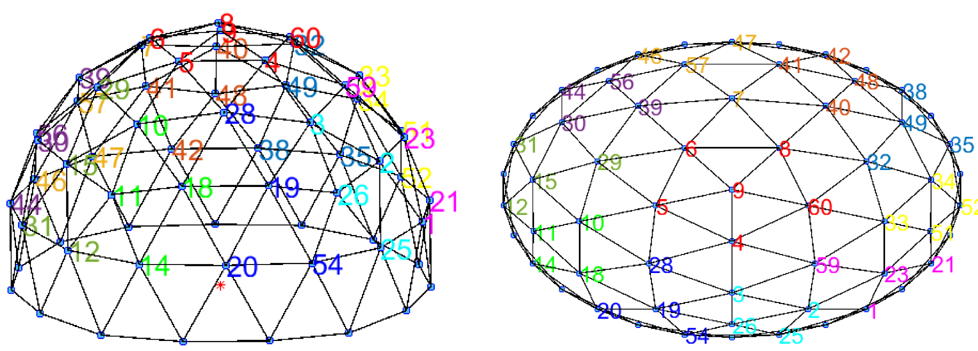

Figure 20: Impact locations including 11 zones: elevation view and plan view

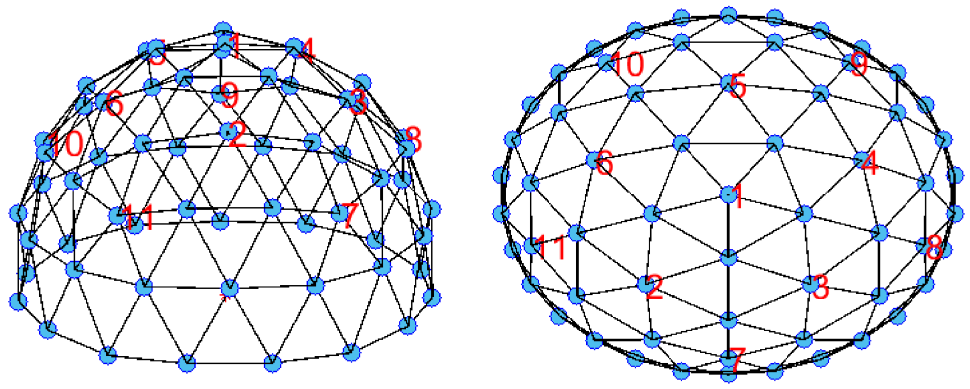

Figure 21: Impact measurement including 11 accelerometers: elevation view and plan view

4.2. Impact detection and localization for each sensor

The proposed method is applied to this case study, where impact detection is first applied; impact localization is then triggered if the detection result is positive. This process takes place in each sensor, which is illustrated in this section, and then information fusion is conducted afterward, which will be presented in the next section.

To evaluate the impact detection strategy described in Section 2.2 and 2.3, each of the eleven sensors was examined using the impact simulation results obtained in Section 4.1. In each impact simulation, data cleansing using wavelet denoising is first employed, and the curve fitting of data envelopes is triggered if the cleansed record exceeds $0.1g$. Only if the obtained exponential index is larger than the threshold of 5, the event is considered as an impact, indicating the impact detection result as 1; otherwise, the result is 0. Fig. 22 illustrates the detection results of Sensor 1, 5, and 9. Taking Sensor 1 as an example, if the noise level is low (i.e., -55dB), the impact detection accuracy is always 100%. As the noise level increases, the impact detection accuracy is relatively low for minor impacts but becomes high for moderate/strong impacts. Similar patterns can also be observed for the other two sensors in the figure.

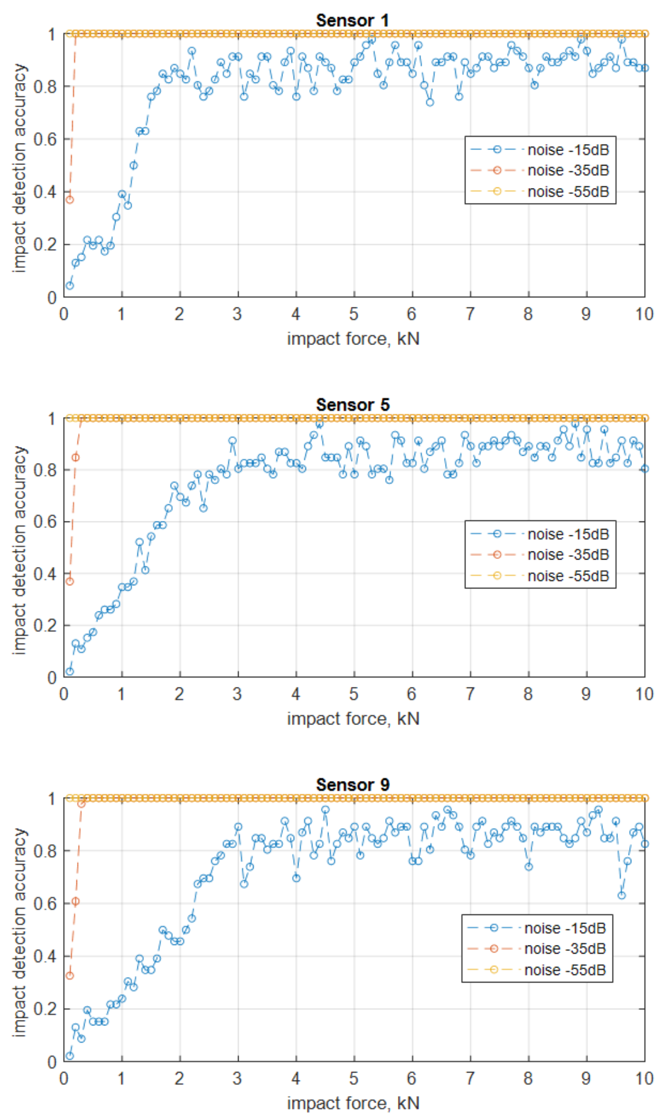

Figure 22: Impact detection results: (a) Sensor No.1, (b) Sensor No.5, and (c) Sensor No.9

Afterward, the impact localization strategy is carried out for each sensor node, if the impact detection result is positive. In this case study, the CNN model described in Fig. **??** is also employed for impact localization, where the number of feature learning layers is 12 for this complex structure. The database obtained in Section 4.1 is divided into three parts, where 60% datasets are used for training, 20% for validation, and 20% for testing. The localization accuracy for each of the eleven sensor nodes is plotted in Fig. 23. It can be seen that, most sensor nodes can achieve relatively high precision of above 60% for impact localization if noise is not introduced. However, only Sensor 1 has an extremely low accuracy of 28.3%. Based on the confusion matrix in Fig. 24a, Zone 1 has an accuracy of 100%, but all other zones have very low accuracies. This is due to the symmetric characteristics of

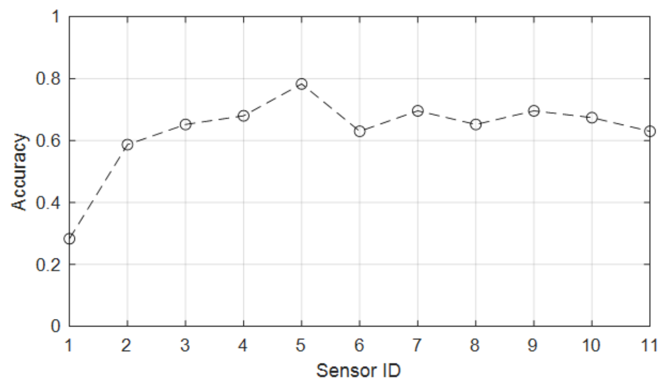

Figure 23: Impact detection and localization results for each sensor

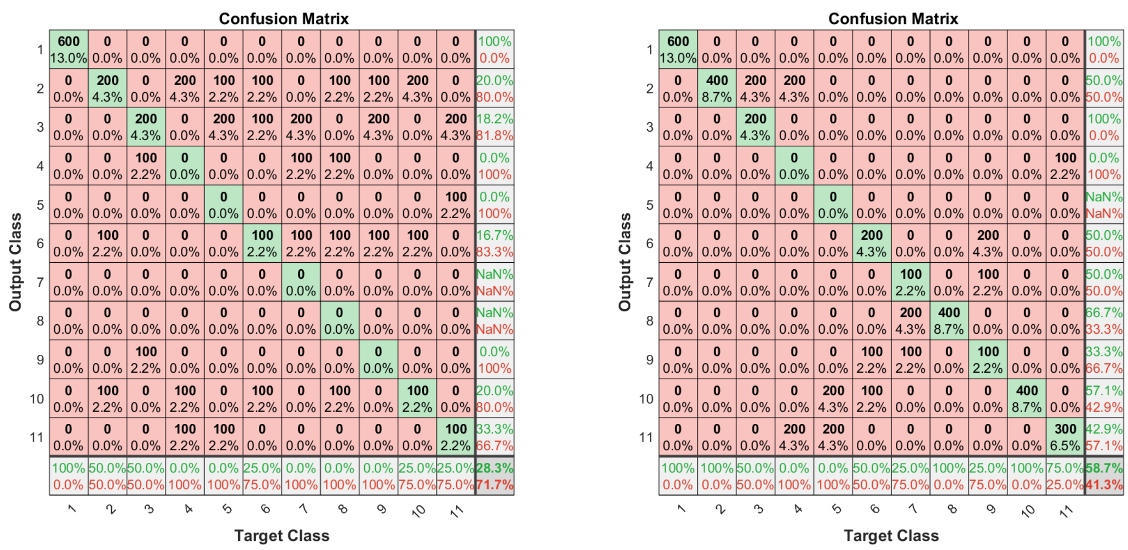

(a) (b)

Figure 24: Impact localization results: (a) Sensor No.1, and (b) Sensor No.2

the dome structure. Zone 1 is in the middle of the dome structure, whereas other zones are difficult for Sensor 1 to differentiate from one to the symmetric counterpart. The results can help to exclude this position if limited sensors are deployed. Similarly, the confusion matrix in Fig. 24b can be further explained considering the symmetric properties of the structure, as shown in Fig. 25. In particular, impacts happening in Zone 4 are all mistakenly classified as either in Zone 2 or in Zone 11. In sum, the above results can lead to two conclusions as follows: 1) as the initial step of our proposed strategy, the impact localization of each sensor can compare their performance individually and hence facilitate the optimal sensor placement; 2) due to the symmetries and other complex behaviors, a single sensor node alone may not be sufficient for effective impact localization, calling for the usage of information fusion (as discussed in the following section).

4.3. Information fusion results and discussions

To fully evaluate the efficacy of information fusion (i.e., combining information from more than one sensor), we introduce measurement errors and modeling errors for each impact simulation. Then, impact localization accuracy is compared between different fusion scenarios under different conditions.

As shown in Fig. 26, it can be seen that the impact localization accuracy for each sensor alone decreases, as the noise floor increases. This observation is applicable to all the sensor nodes but with different levels of accuracy drops. If the noise floor increases to -15dB, the impact localization results are not acceptable if using a single sensor, dropping below 50%, calling for information fusion of multiple sensors. To examine the effects of information fusion (as described in Section 2.5), two strategies are applied. Firstly, Sensor 1 is used as the starting point and gradually combined with Sensor 2, 3, 4, and 5, respectively. In total, five stages of information fusion are compared. The purpose is to check the efficacy of the information fusion, even though a relatively bad sensor location is included. The impact localization accuracy for each stage of information fusion is plotted in Fig. 27a. It can be seen that, although the starting stage has relatively low accuracy, adding one more sensor

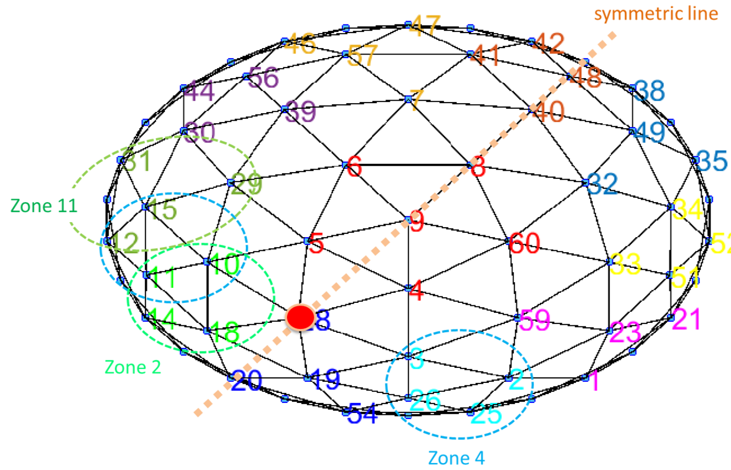

Figure 25: Impact zone symmetries for Sensor No.2

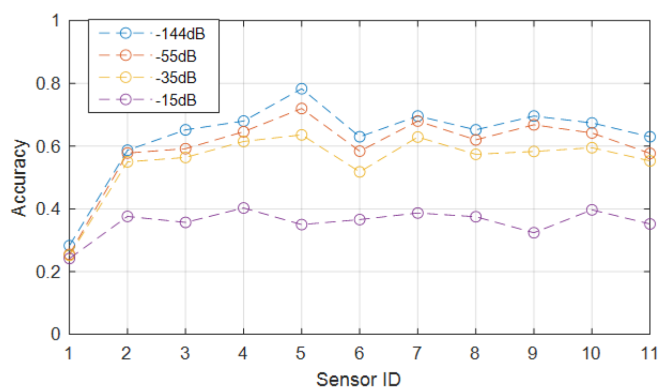

Figure 26: Impact detection and localization accuracy with measurement errors

information can significantly improve the results under different noise floors, combating the influences of noises. Adding more sensors can further increase the accuracy but the margin of benefits is reduced gradually, converging to a certain value. For relatively low noise levels, only three sensors are needed to achieve an accuracy of close to 100%. Secondly, based on the findings in Fig. 23, we exclude Sensor 1 and select optimal sensors. In particular, we start from Sensor 4 and add Sensor 5, 6, 7, and 8, gradually, as each of the five stages for information fusion. The purpose is to check the best efficacy of the information fusion with optimal sensor placements. As shown in Fig. 27b, we can see that, for relatively low noise levels, only two sensors are required to achieve an accuracy of close to 100%.

A similar evaluation is conducted for the examination of the effects of modeling errors. Using Eq. 15, different magnitudes of modeling errors are established and a corresponding database is built for the testing of impact localization. As shown in Fig. 28, as the modeling error increases, the accuracy of impact localization decreases for each sensor node, calling for information fusion. To do this, we also explore two strategies, including 1) a combination of Sensor 1, 2, 3, 4, and 5, and 2) a combination of Sensor 4, 5, 6, 7, and 8. It can be concluded

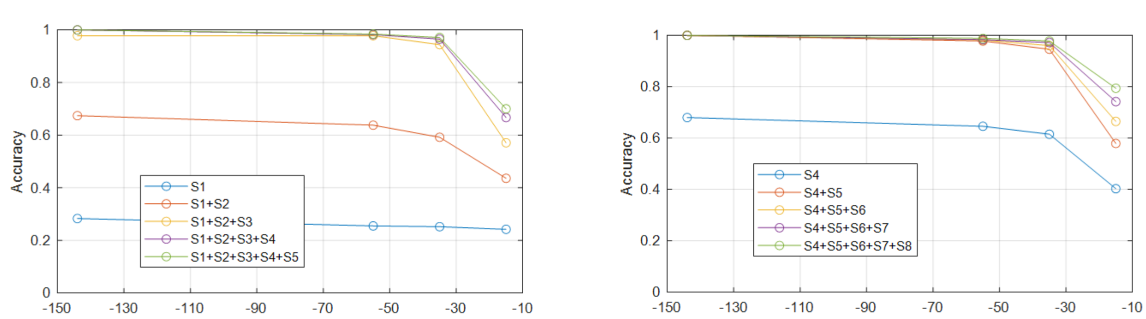

(a) (b)

Figure 27: Impact localization results with measurement errors: (a) fusion strategy 1, and (b) fusion strategy 2

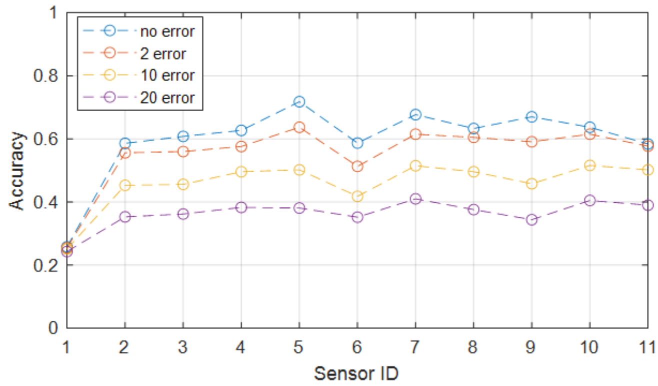

Figure 28: Impact detection and localization accuracy with modeling errors

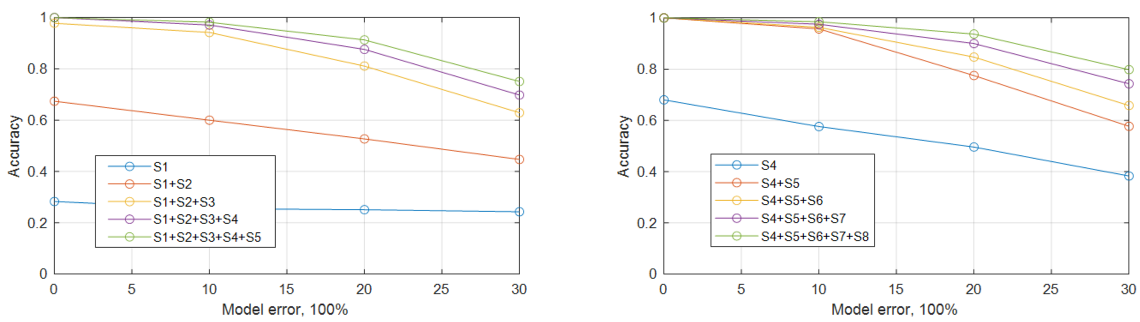

Figure 29: Impact localization results with modeling errors: (a) fusion strategy 1, and (b) fusion strategy 2

that information fusion can help to increase the accuracy of impact localization at different levels of modeling errors, combating the influences of modeling errors. While including a relatively bad sensor position, three sensors are required to achieve a satisfactory accuracy of impact localization. For optimal sensor placements, the desired number of sensor nodes can be reduced to two.

In sum, the case study results demonstrate that, as long as one sensor survives under impacts, the impact detection and localization results are acceptable. If more sensors are included for information fusion, higher accuracy can be achieved, revealing the scalability, efficacy and robustness of our proposed strategy.

5. Concluding Remarks

This paper presents a novel strategy for impact detection and localization using signal processing, deep learning, and information fusion. It is robust and scalable, suitable for harsh environments (e.g., deep space habitats) where sensors may be damaged under impact events. It is also effective for stiff structures, under either measurement errors or modelling errors. In particular, an effective data cleansing and envelope curve fitting strategy is proposed to detect the event of impacts with high accuracy, using noisy measurement data. Convolutional neural networks are trained for each sensor node and are fused using Bayesian theory to improve the accuracy of impact localization. Such an arrangement can not only help to optimally select sensor locations and sensor numbers, but also help to mitigate the adverse effects of measurement errors and modeling errors. The proposed strategy has been illustrated using a 1D structure numerically and demonstrated using a 3D geodesic dome structure, considering the uncertainties of measurement errors and modeling errors.

6. Acknowledgements

The authors gratefully acknowledge the support of this research by a Space Technology Research Institutes Grant (number 80NSSC19K1076) from NASA's Space Technology Research Grants Program, the start-up grant at Nanyang Technological University, Singapore (03INS001210C120), and the Ministry of Education Tier 1 Grants, Singapore (No. RS121/21).

References

[1] U. Polimeno, M. Meo, Detecting barely visible impact damage detection on aircraft composites structures, Composite Structures (2009). doi:10.1016/j.compstruct.2009.04.014.

[2] A. C. Garner, W. A. Huff, The wreck of Amtrak's Sunset Limited: News coverage of a mass transport disaster, Disasters (1997). doi:10.1111/1467-7717.00041.

[3] E. M. Merlo, A. Bulletti, P. Giannelli, M. Calzolai, L. Capineri, A novel differential time-of-arrival estimation technique for impact localization on carbon fiber laminate sheets, Sensors (Switzerland) (2017). doi:10.3390/s17102270.

[4] B. W. Jang, C. G. Kim, Acoustic emission source localization in composite stiffened plate using triangulation method with signal magnitudes and arrival times, Advanced Composite Materials (2020). doi:10.1080/09243046.2020.1786903.

[5] E. Kirkby, R. de Oliveira, V. Michaud, J. A. Månson, Impact localisation with FBG for a self-healing carbon fibre composite structure, Composite Structures (2011). doi:10.1016/j.compstruct.2011.07.030.

[6] T. Kundu, X. Yang, H. Nakatani, N. Takeda, A two-step hybrid technique for accurately localizing acoustic source in anisotropic structures without knowing their material properties, Ultrasonics (2015). doi:10.1016/j.ultras.2014.08.009.

[7] T. Kundu, Acoustic source localization, 2014. doi:10.1016/j.ultras.2013.06.009.

[8] Q. Li, Q. Lu, Impact localization and identification under a constrained optimization scheme, Journal of Sound and Vibration (2016). doi:10.1016/j.jsv.2015.12.010.

[9] B. T. Davis, J. M. Caicedo, V. A. Hirth, Force Estimation and Event Localization (FEEL) of Impacts Using Structural Vibrations, Journal of Engineering Mechanics (2021). doi:10.1061/(asce)em.1943-7889.0001890.

[10] G. Yan, H. Sun, O. Büyüköztürk, Impact load identification for composite structures using Bayesian regularization and unscented Kalman filter, Structural Control and Health Monitoring (2017). doi:10.1002/stc.1910.

[11] M. M. Saleem, H. Jo, Impact force localization for civil infrastructure using augmented Kalman Filter optimization, Smart Structures and Systems (2019). doi:10.12989/sss.2019.23.2.123.

[12] P. Shrestha, J. H. Kim, Y. Park, C. G. Kim, Impact localization on composite wing using 1D array FBG sensor and RMS/correlation based reference database algorithm, Composite Structures (2015). doi:10.1016/j.compstruct.2015.01.029.

[13] M. S. Hossain, Z. C. Ong, Z. Ismail, S. Y. Khoo, A comparative study of vibrational response based impact force localization and quantification using radial basis function network and multilayer perceptron, Expert Systems with Applications (2017). doi:10.1016/j.eswa.2017.05.027.

[14] B. W. Jang, C. G. Kim, Impact localization of composite stiffened panel with triangulation method using normalized magnitudes of fiber optic sensor signals, Composite Structures (2019). doi:10.1016/j.compstruct.2019.01.028.

[15] L. Morse, Z. Sharif Khodaei, M. H. Aliabadi, Reliability based impact localization in composite panels using Bayesian updating and the Kalman filter, Mechanical Systems and Signal Processing (2018). doi:10.1016/j.ymssp.2017.05.047.

[16] I. Tabian, H. Fu, Z. S. Khodaei, A convolutional neural network for impact detection and characterization of complex composite structures, Sensors (Switzerland) (2019). doi:10.3390/s19224933.

[17] Z. Sharif-Khodaei, M. Ghajari, M. Aliabadi, Determination of impact location on composite stiffened panels, Smart Materials and Structures 21 (2012) 105026.

[18] C. E. Silva, D. Gomez, A. Maghareh, S. J. Dyke, B. F. Spencer Jr, Benchmark control problem for real-time hybrid simulation, Mechanical Systems and Signal Processing 135 (2020) 106381.